

# Plasma detachment mechanisms in a magnetic nozzle

M. Merino\* and E. Ahedo†

*Universidad Politécnica de Madrid, 28040 Madrid, Spain*

An axisymmetric model of the supersonic expansion of a collisionless, totally ionized plasma in a divergent magnetic nozzle and the DIMAGNO simulation code are being used to study the plasma detachment from the guiding magnetic field, taking into account the effects of the induced magnetic field generated by the plasma electric currents. The azimuthal electric currents carried by the plasma from the discharge chamber or created within the nozzle are the central feature for both thrust generation and plasma detachment. These currents are mainly electronic and have a globally diamagnetic character, as their induced field lowers the total field around the axis and increases nozzle divergence rate. This paper focuses on the role of the plasma-generated magnetic field and the detachment issue, particularized for the case of a helicon thruster (although conclusions extracted herein might be easily generalizable to other thruster types). A viable alternative detachment mechanism based on plasma self-demagnetization is investigated.

## I. Introduction

Propulsive Magnetic Nozzles (PMN) are the fundamental acceleration device of advanced plasma thrusters currently being developed. PMN are being used to guide, control and accelerate a plasma beam in the helicon thruster,<sup>1-4</sup> the VASIMR,<sup>5</sup> and the Applied-Field MagnetoPlasmaDynamic Thruster.<sup>6</sup> It is also a secondary element of the Diverging Cusped Field Thruster<sup>7</sup> and some configurations of the Cylindrical Hall Thruster.<sup>8</sup>

The fundament of these devices lies on the possibility of controlling the expansion of a plasma into vacuum with an imposed magnetic field of appropriate geometry and mild intensity, strong enough to have electrons magnetized. Accomplishing this allows to nozzle the plasma without magnetizing ions—which would require a magnetic field several orders of magnitude stronger,—since electrons pull ions via the ambipolar electric field that ensues. A PMN exhibits a thermoelectric character, as it converts the thermal energy present in the plasma (provided electrically by the plasma source) into directed kinetic energy of ions, in close resemblance to a traditional de Laval nozzle with a supersonic neutral gas.<sup>9</sup> On the other hand, the PMN can be termed a electromagnetic device, since the external forces that channel the plasma and convey the produced thrust back to the engine are purely magnetic.

The discussion presented in this paper is based on the two-dimensional, two-fluid model of a collisionless, quasineutral and totally-ionized plasma flow in a divergent PMN introduced in Ref. 10. The model assumes that electrons are fully magnetized, and allows any degree of ion magnetization. This is typically the situation with the helicon thruster, which consists of a helicon plasma source ending in a PMN, such as the HPH.com thruster being developed in Europe.<sup>4</sup> In a helicon source, most of the energy is deposited on the electrons, while ions remain relatively cold. A plasma with these characteristics constitutes the reference case for this study, although most of the results obtained therewith are readily generalizable or adaptable to more complex plasmas.

With the help of this model, we performed a parametric investigation of the evolution of the plasma in the PMN and characterized its propulsive performances when the plasma density is low enough to neglect the induced magnetic field it creates, i.e., when the plasma beta,  $\beta = \mu_0 n T_e / B^2 \ll 1$ . We showed that the confinement and acceleration of the plasma is governed by the presence of azimuthal electric currents in the plasma, which (1) are mainly electron-based, (2) possess a globally diamagnetic character with respect to the external magnetic field in order to produce thrust and (3) are proportional to the internal energy of

\*Student, AIAA Student Member (mario.merino@upm.es)

†Professor, AIAA Member

the plasma. When cold ions do not rotate initially their contribution to azimuthal currents is paramagnetic, which was found to be negligible for the parametric range explored (at least up to the magnetic nozzle turning point). It was seen that the plasma response is strongly 2D, and that many important aspects such as these azimuthal electric currents, or the not-fulfillment of local current ambipolarity in the longitudinal plane, are only recoverable with a two-dimensional model.

Building upon these results, a preliminary investigation of the issue of plasma detachment from the applied field was carried out in Refs. 11,12. The relevance of achieving plasma detachment in a PMN once it has been accelerated arises in the closed nature of magnetic streamlines, which poses a major concern about the use of PMN for space propulsion. Without proper separation from the field, the magnetized plasma would return onto the thruster along field lines, ruining thrust and endangering sensitive spacecraft surfaces and equipment. A competitive PMN requires the bulk of the plasma to detach well before the turning point of the magnetic lines, keeping attachment losses (which might be unavoidable) to a minimum.

Arguably, the ability of a mild magnetic field to deflect 180 deg an energetic plasma beam must be limited. However, the mechanisms that allow the plasma to detach are complex and controversial, and they are still not well understood. A number of detachment theories have been proposed in the last years: firstly, it has been claimed that plasma electric currents could be strong enough to modify the geometry of the magnetic field and stretch the magnetic lines to infinity, effectively avoiding the problem of detachment, as the plasma would carry the magnetic field with it instead of turning back.<sup>13</sup> However, as we demonstrated in Ref. 12, this scenario implicitly requires the azimuthal currents to be *paramagnetic* so that plasma-induced magnetic field reinforces the applied one axially and avoids the magnetic lines to turn back. This is unfortunately not the case for a PMN, where the azimuthal plasma currents are dominantly *diamagnetic* at least up to the turning point.

Secondly, plasma resistivity<sup>14</sup> and electron inertia effects,<sup>15</sup> although small in the largest part of the plasma volume, have also been proposed as plausible detachment mechanisms, which would allow electrons to diffuse across the magnetic field lines, allowing the plasma beam to continue its downstream motion without turning back. However, we have shown that these diffusive-detachment mechanisms lead to *divergent detachment* in a PMN, meaning that the plasma plume would diverge faster than the magnetic field, which is an undesired situation. It follows that resistivity (and electron inertia) effects should be kept to a minimum to avoid the additional, uncontrolled plasma divergence. The reason why these detachment mechanisms produce divergent detachment is again related to the plasma currents being diamagnetic.

The diamagnetic nature of the plasma has been recently confirmed experimentally.<sup>16</sup> Indeed, the applied and the induced magnetic fields need to repel each other to produce thrust, requiring a diamagnetic character of the latter.

Two new detachment mechanisms which do observe this requirement for thrust were suggested in Ref. 12. Firstly, it is observed from the simulations that for low ion magnetization, the plasma near the vacuum becomes strongly rarefied, as most of the ion flux diverges much less than the magnetic field. This is a consequence of ions being already detached from the field and the ambipolar electric field not being able to significantly alter their trajectories without further rarefaction. This is highly beneficial for propulsion, as radial efficiency losses are kept much lower than if ions followed magnetic lines, and it can be regarded as a naturally-occurring *self-separation* detachment. Related to this, an interesting possibility to be explored is the appearance of non-neutral effects due to the low density near the plasma-vacuum transition, which could participate in the development of the plasma-vacuum edge and allow its detachment from the field.

The second plausible detachment mechanism is plasma demagnetization fostered by the self-induced field. This *self-demagnetization* detachment is motivated again by the diamagnetic character of the plasma currents: the induced magnetic field that they create competes with the applied one, lowering the intensity of the field downstream. If conditions are appropriate, the resulting magnetic field might become weak enough for electrons to become unmagnetized, meaning that plasma would be able to detach from the magnetic field.

This paper is dedicated to the investigation of the second detachment mechanism. The model of Ref. 10 is extended to include the induced magnetic field as described in section II, in order to allow the study of plasma flows with  $\beta > 0$ . The self-consistent magnetic field is calculated with an iterative method. Then, section III presents the simulation results for the induced magnetic field and derived quantities, which provide the necessary elements for the discussion of detachment in section IV. There, the self-separation and self-demagnetization mechanisms are analyzed within the limits of the present model. Finally, the main conclusions of this work are gathered in section V. An appendix details the procedure used to calculate the

applied and induced magnetic fields.

## II. Plasma model and integration

The 2D model developed in Ref. 10 is extended here to include the induced magnetic field. A quasineutral, collisionless plasma, formed by cold ions and hot Maxwellian, isothermal electrons ( $T_e = \text{const}$ ), streaming out of an helicon source at ion-sonic velocity, is subject to the action of a total magnetic field  $\mathbf{B} = \mathbf{B}_a + \mathbf{B}_p$ , resulting from the superposition of an applied, external magnetic field  $\mathbf{B}_a$ , and the plasma-induced magnetic field  $\mathbf{B}_p$  created by the electric currents present in the plasma. It is assumed that electron inertia plays a negligible role, and that electrons are completely magnetized so that they remain in their initial streamtube ( $\mathbf{u}_e = u_{\parallel e} \mathbf{1}_{\parallel} + u_{\theta e} \mathbf{1}_{\theta}$ , with  $\mathbf{1}_{\parallel}$  and  $\mathbf{1}_{\theta}$  the unit vectors in the direction parallel to  $\mathbf{B}$  and the azimuthal direction. Analogously,  $\mathbf{1}_{\perp} = \mathbf{1}_{\theta} \times \mathbf{1}_{\parallel}$  is defined). The equations that govern the flow,<sup>10</sup> expressed in cylindrical coordinates  $(z, r, \theta)$  centered at the nozzle throat, are summarized below:

$$u_{zi} \frac{\partial \ln n}{\partial z} + u_{ri} \frac{\partial \ln n}{\partial r} + \frac{\partial u_{zi}}{\partial z} + \frac{1}{r} \frac{\partial (ru_{ri})}{\partial r} = 0, \quad (1)$$

$$u_{zi} \frac{\partial u_{zi}}{\partial z} + u_{ri} \frac{\partial u_{zi}}{\partial r} + c_s^2 \frac{\partial \ln n}{\partial z} = -(u_{\theta i} - u_{\theta e}) B_r, \quad (2)$$

$$u_{zi} \frac{\partial u_{ri}}{\partial z} + u_{ri} \frac{\partial u_{ri}}{\partial r} + c_s^2 \frac{\partial \ln n}{\partial r} = (u_{\theta i} - u_{\theta e}) B_z + \frac{u_{\theta i}^2}{r}, \quad (3)$$

$$rm_i u_{\theta i} + e\psi = D_i(\psi_i), \quad (4)$$

$$T_e \ln n - e\phi = H_e(\psi), \quad (5)$$

$$u_{\theta e} = -\frac{r}{e} \frac{\partial H_e}{\partial \psi}, \quad (6)$$

$$\frac{nu_{\parallel e}}{B} = G_e(\psi). \quad (7)$$

The longitudinal components of the different magnetic fields can be expressed through a streamfunction  $\psi_k$ , where the subindex  $k$  indicates the applied ( $a$ ), plasma ( $p$ ) and total (no subindex) fields, with

$$\frac{\partial \psi_k}{\partial r} = rB_{zk}; \quad \frac{\partial \psi_k}{\partial z} = -rB_{rk}. \quad (8)$$

Equations 1–7 need to be complemented with Ampère's equation in order to include the induced magnetic field:

$$\nabla \times \mathbf{B}_p = \mu_0 (\mathbf{j}_i - \mathbf{j}_e) = \mu_0 en (\mathbf{u}_i - \mathbf{u}_e). \quad (9)$$

In the previous equations  $c_{si} = \sqrt{T_e/m_i}$  is the sound velocity of ions, and  $D_i(\psi_i)$ ,  $H_e(\psi)$ ,  $G_e(\psi)$  are functions of the ion streamline function  $\psi_i$  and total magnetic field streamfunction  $\psi$  that can be evaluated given the initial conditions. These expressions can be normalized using  $T_e$  (electron temperature, energy units),  $m_i$  (ion mass),  $e$  (element charge),  $R$  (plasma radius at nozzle throat) and  $n_0$  (plasma density at the centerline at the throat). A hat is used to denote dimensionless variables, e.g.  $\hat{\phi} = e\phi/T_e$ ,  $\hat{B} = eRB/\sqrt{T_e m_i}$ ,  $\hat{n} = n/n_0$ . Notice that Eq. 9 can then be re-written as

$$\nabla \times \hat{\mathbf{B}}_p = \beta_0 \hat{B}_{a0}^2 \hat{n} (\hat{\mathbf{u}}_i - \hat{\mathbf{u}}_e), \quad (10)$$

where  $\beta_0 = \mu_0 n_0 T_e / B_{a0}^2$  is the plasma beta at the origin.

Aside from the geometry of the imposed magnetic field  $\mathbf{B}_a$  (here created by a set of two solenoids, as detailed in the appendix, the resulting model depends on (1) the magnitude of this field at the origin,  $B_{a0}$ , which controls the degree of ion magnetization. Notice that  $\hat{B}_{a0} \simeq \hat{B}_0 = \hat{\Omega}_{i0} = R\Omega_{i0}/c_s$ , the dimensionless ion gyrofrequency at the origin. A typical helicon xenon thruster with  $R = 10$  cm,  $T_e = 20$  eV and  $B_{a0} = 200$  G has  $\hat{B}_{a0} = 0.38$ . For practical devices,  $\hat{B}_{a0}$  is expected to range from 0.1 or lower to 1 (Refs. 2, 3). Additionally, the plasma response is dependent on (2) the plasma density, electric potential, and velocity profiles at the nozzle throat, and (3)  $\beta_0$ , which determines the relative importance of the induced magnetic field with respect to the applied one. In previous work, it was assumed that  $\beta_0 \ll 1$ , and the induced magnetic field effects were neglected.

In this article, we are concerned with the role of the induced magnetic field in the plasma response, which is governed by  $\beta_0$ . The influence of ion magnetization and plasma profiles was already studied in Ref. 10; therefore, for the present study, simulations will use  $B_{a0} = 0.1$  and the non-uniform density profile characteristic of helicon sources described in the mentioned reference.

Inclusion of the elliptic Ampère’s equation (Eq. 10) ruins the hyperbolic character of Eqs. 1–3, upon which our solution method is based. To deal with this, a new iterative scheme to obtain the self-consistent solution of the plasma response with the induced magnetic field that it generates has been implemented into a new version of our DIMAGNO code,<sup>10,17</sup> which has been restructured into a new object-oriented architecture for improved flexibility (OO-DIMAGNO). The ability to calculate the induced magnetic field frees the previously-existing constrain of  $\beta_0 \ll 1$  that assured a negligible induced field.

The scheme is based on solving the plasma and the magnetic field separately. Firstly, the plasma response for a fixed magnetic field, which initially is just the applied field  $\mathbf{B}_a$ , is obtained. Taking advantage of the supersonic character of the plasma flow, equations 1–7 are numerically integrated with the Method of Characteristics (MoC), which reduces the partial differential equations (Eqs. 1–3) to ordinary differential equations along the three families of characteristic lines in the meridian plane of the nozzle (two Mach line families and the ion streamlines). Adequate propagation and intersection of these characteristics allows then to calculate the plasma response. This makes DIMAGNO a fast and accurate code for calculating the plasma response in the PMN, displaying greater performances than other finite difference schemes.<sup>18,19</sup>

Knowing this first version of the plasma flow, the induced field  $\mathbf{B}_p^1$  due to the plasma electric currents is calculated. This field is then used to correct the total field of the next iteration,  $\mathbf{B} = \mathbf{B}_a + \mathbf{B}_p^1$ . A new induced field results from this iteration,  $\mathbf{B}_p^2$ . This iterative process is repeated until convergence of the induced magnetic field  $\psi_p$  function is reached everywhere in the computational domain. The solutions obtained in this way readily converge to the self-consistent flow and magnetic field (absolute error in  $\psi_p/B_{a0}$  diminishes about one order of magnitude per iteration for small values of  $\beta_0$ ). A detailed description of the calculation of the applied and induced magnetic field is described in the appendix.

### III. Induced magnetic field

Diamagnetic azimuthal currents are a key element of a PMN, as they produce the radial confining force  $j_\theta B_{za} < 0$  that compensates for the radial pressure gradient  $-T_e \partial \ln n / \partial r > 0$ , but also the axial accelerating force  $-j_\theta B_{ra} > 0$ . As shown in Eq. 17 of the appendix, these forces are proportional to  $j_\theta B_{a0} \sim T_e$ , which manifests that propulsive performances largely depend on the internal energy. An intuitive way to express this is that the plasma pressure “pushes” against the magnetic field lines as if they were the virtual walls of a solid nozzle, so that the expansion is directed mostly axially, producing thrust. For the same reasons, the presence of paramagnetic currents is detrimental for propulsion.

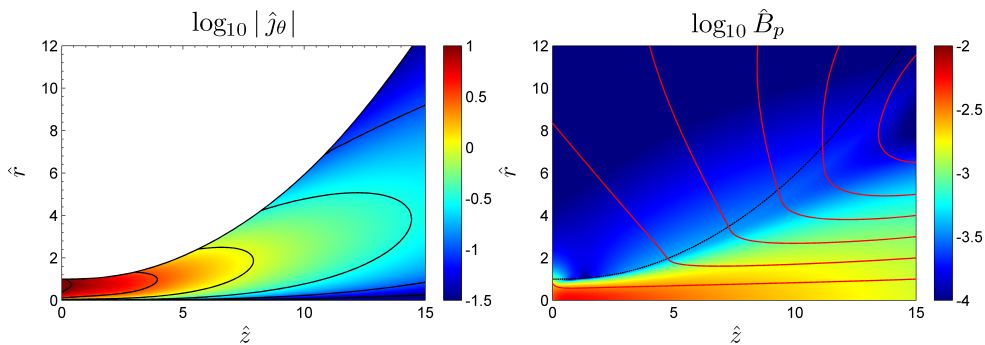


**Figure 1.** Magnitude of the azimuthal currents (left),  $\log_{10} |\hat{j}_\theta|$  and their induced magnetic field (right) when  $\beta_0 = 0.1$ . The currents are diamagnetic ( $j_\theta < 0$  for  $B_{za} > 0$  at the axis). Black contour lines in steps of 0.5 of the magnitude  $\log_{10} |\hat{j}_\theta|$  are displayed. Red lines show the direction of the induced magnetic field, which opposes the applied one at the axis. Plasma-vacuum line (dashed black) has been plotted for reference.

As explained in the previous section, these currents give rise to a longitudinal induced magnetic field, which opposes the applied one. Azimuthal plasma currents and their induced field are shown in figure 1 for a representative case. It is seen that  $j_\theta$  is larger closer to the nozzle throat, and diminishes as the plasma

expands downstream. The induced magnetic field is stronger about the nozzle centerline, and its direction is almost-axial in most of the plasma domain.

The consequences of this induced field are twofold: (1) the opening of the magnetic streamtubes (producing a faster-diverging nozzle) and (2) the weakening of the total field. Figure 2 shows the magnitude of these effects in the total magnetic field for different values of  $\beta_0$ . These results agree qualitatively with the predictions of a previous first-order perturbation analysis.<sup>11</sup>

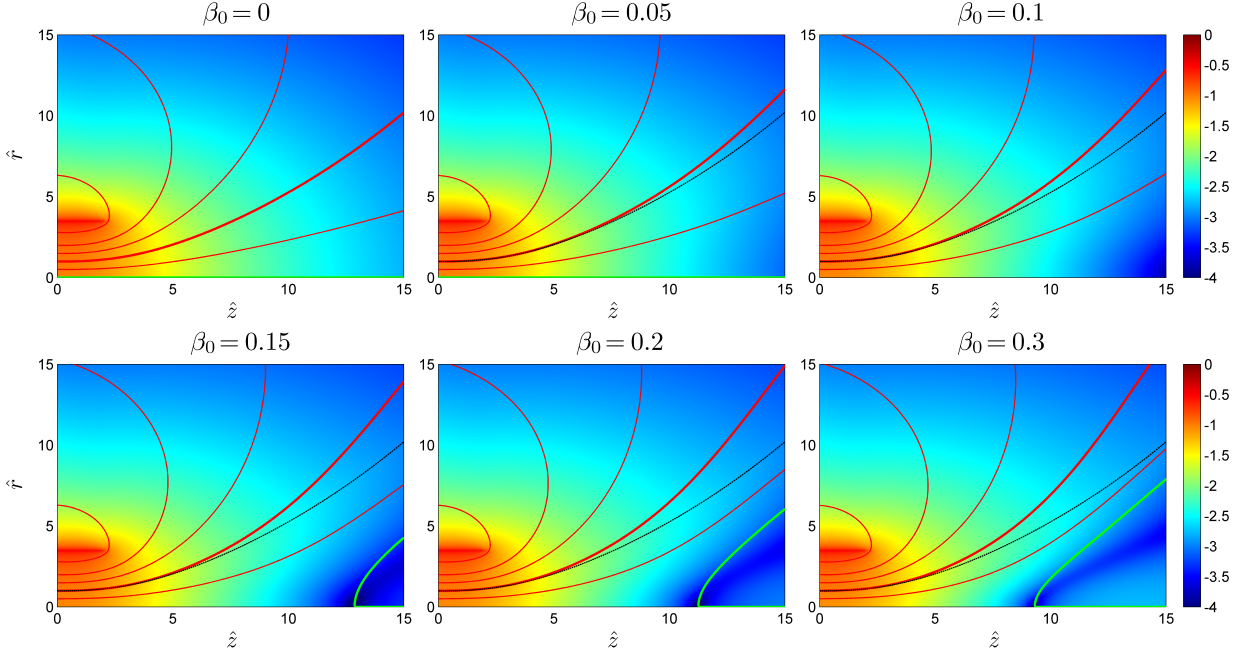


**Figure 2.** Self-consistent total magnetic field  $B = B_a + B_p$  for different values of  $\beta_0$ . The background color indicates the intensity of the field in logarithmic scale,  $\log_{10} \hat{B}$ . Red lines show magnetic streamlines, the thicker one being the plasma-vacuum edge in the simulations (it passes through  $\hat{z} = 0, \hat{r} = 1$ ). The black dashed line serves to compare this to the corresponding line of the initial applied magnetic field,  $B_a$ . The green line, when present, displays the magnetic separatrix,  $\psi = 0$ .

These results show that larger values of  $\beta_0$  cause weaker total magnetic fields downstream. An interesting feature of these figures is the existence of a region of very low magnetic field around the axis, that moves upstream as  $\beta_0$  increases. This hints that the induced magnetic field can become an outstanding mechanism to lower the total field magnitude enough to allow electron demagnetization for moderate  $\beta_0$ . Additionally, some of the simulations exhibit a saddle-point within this zone where the field actually cancels out, followed by a separatrix surface that extends downstream and divides the magnetic field in two disconnected regions, *internal* (upstream) and *external* (downstream). The existence of a point where  $B = 0$  has been observed in recent experiments by Roberson *et al.*<sup>16</sup> Since our current model cannot predict the electron currents that might exist beyond the separatrix line (where  $\psi < 0$ ), we have taken  $j_{\theta e} = 0$  in this region. The actual magnetic field may therefore differ in this zone and its neighborhood for the simulations with larger  $\beta_0$ . We are currently working to properly model flow and currents in the demagnetized plasma.

The strong alteration of the geometry and intensity of the magnetic nozzle seen in figure 2 has profound implications in the behavior of the plasma and its detachment from the field: firstly, thruster performances are affected. The additional divergence of the field causes a decrease of the plume efficiency  $\eta_{plume}$ , which quantifies the radial kinetic losses,<sup>10</sup>

$$\eta_{plume}(z) = \frac{P_{zi}(z)}{P_i(z)} = \frac{\int_{A(z)} m_i n u_{zi}^3 / 2 dA}{\int_{A(z)} m_i n u_i^2 u_{zi} / 2 dA}, \quad (11)$$

where  $P_{zi}(z)$  and  $P_i(z)$  are, respectively, the ion axial and total power traversing section  $A(z)$  (plane perpendicular to the axis at position  $z$ ). Figure 3 displays (1) the thrust gain  $\kappa_{noz}(z) = F(z)/F(0) - 1$ ,

with  $F(z) = \int_{A(z)} (nu_{zi}^2 + nT_e) dA$  the thrust (ion momentum plus electron pressure) achieved at section  $A(z)$ , and (2) the plume efficiency  $\eta_{plume}(z)$  for different values of  $\beta_0$ . These results manifest that while  $\kappa_{noz}$  remains almost unaffected (although a small decrease for the same nozzle aperture  $\hat{r}$  seems to occur),  $\eta_{plume}$  decreases as  $\beta_0$  increases.

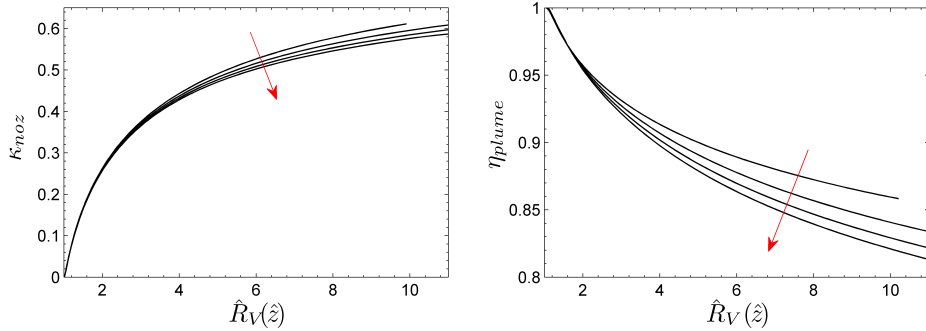


**Figure 3.** Nozzle performances  $\kappa_{noz}(z)$  (left) and  $\eta_{plume}(z)$  (right) plotted against the value of the nozzle radius  $R_V$  at that each  $z$ -section, for  $\beta_0 = 0, 0.05, 0.1$  and  $0.15$  (direction of increasing values of  $\beta_0$  denoted with arrows).

Secondly, as the plasma moves downstream, it approaches the low- $B$  region and the separatrix surface. There, the plasma near the axis and the plasma near the nozzle edge can behave differently. The weaker field near the axis enhances demagnetization of electrons, which become effectively free of the influence of the applied magnetic field, and thus are able to traverse the separatrix surface and continue downstream. Subsequent development of the plasma beam is then dominated by the residual plasma pressure and plasma currents/induced field. The flow thereafter might then be described in an approximate way with e.g. self-similar plasma plume expansion models.<sup>20</sup>

On the other hand, the influence of the induced magnetic field near the nozzle edge is modest, and depending on the plasma properties,  $B$  might be still strong enough for electrons to remain attached. Since the topology of the magnetic field near the separatrix is severely altered, electrons which are unable to traverse this feature will be pulled outwards by the deflected magnetic streamlines. The large slip between ion and electron velocities in this region could give rise to considerable longitudinal currents that might further complicate the flow.

The transition from one behavior to the other, and the plasma dynamics in the external magnetic field behind the separatrix, cannot be determined with the current model, since it is based upon the assumption of magnetized electrons. However, as discussed in the next section, a first estimation of demagnetization can be performed based on the value of the electron Larmor radius  $\ell_e$ , showing that plasma *self-demagnetization* can be a viable detachment mechanism for the bulk of the plasma beam.

#### IV. Plasma detachment via demagnetization

The model of section II is based upon the fundamental assumption

$$\lambda_D \ll \ell_e \ll R, \quad (12)$$

i.e., that the Debye length  $\lambda_D$  is the smallest scale in the problem, and that electron Larmor radius  $\ell_e$  is smaller than the macroscopic gradient length (which is  $\sim R$ , the initial nozzle radius). As long as this scale ordering is fulfilled, electrons can be assumed to be magnetized, and their movement can be approximately studied with the gyrocenter trajectories, which coincide with magnetic streamlines. This hypothesis might fail due to two reasons. First, for very low plasma densities,  $\lambda_D$  might increase and become  $\lambda_D \sim \ell_e$ , in which case non-neutral effects would strongly alter the orbital motion of electrons about the magnetic streamlines. This phenomenon would destroy their clean helical movement and/or pull their gyrocenters out of their magnetic line, hence producing the demagnetization of electrons. Second, the magnetic field might become low enough to allow  $\ell_e \sim R$ , with the gyroradius becoming of the order of the macroscopic gradient length, resulting in analogous consequences. Here, our attention is focused in this second possibility for attaining demagnetization.

It is important to note that, although ions are normally unmagnetized (their gyrofrequency at the origin,  $\hat{\Omega}_{i0}$ , is typically  $\hat{\Omega}_{i0} \sim 0.1$ –1 or lower in present helicon thrusters), the reason why the plasma remains attached to the magnetic field is the fact that electrons are magnetized, forcing the whole plasma to adapt to the geometry of the magnetic field. Therefore, achieving electron demagnetization is crucial to free the plasma from the field.

Success of the PMN as a plasma accelerator device is conditioned to being able to detach at least the *bulk* of the plasma beam. Fortunately, most of the plasma flux is concentrated about the nozzle axis: there is a strong rarefaction taking place near the plasma edge, related to the *self-separation* of ion and electron streamtubes downstream (illustrated in figure 4). Self-separation<sup>12</sup> is due to ions not being magnetized, and the ambipolar electric field being insufficient to deflect ion trajectories enough (except at the plasma edge to have quasineutrality fulfilled there). This indicates that even in the worst scenario where electrons in the near-edge region remained completely magnetized even after the turning point of magnetic streamlines, they would constitute only a small fraction of the ion flux, and therefore they would not degrade nozzle performances substantially, as long as the core flow is able to detach successfully.

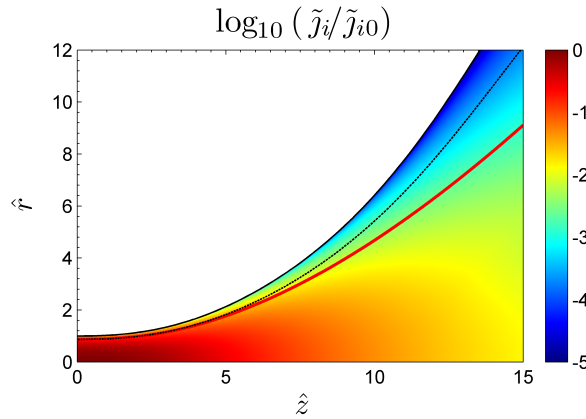


**Figure 4. Logarithm of the ion flux in the longitudinal plane, normalized with its value at the origin  $\log_{10}(\tilde{j}_i/\tilde{j}_{i0})$ , with  $\tilde{j}_i = n\sqrt{u_{zi}^2 + u_{ri}^2}$ . In this simulation,  $\beta_0 = 0.15$ . The streamtube containing 95% of the total ion flux (which passes through  $\hat{r} = 0.86$ ,  $\hat{z} = 0$ ) has been plotted in red. The dashed black line denotes the position of the magnetic streamline that coincides initially with this tube, showing that strong self-separation occurs, and the largest part of the plasma flux does not diverge as much as the magnetic field.**

Having discarded diffusion and field-stretching as viable detachment mechanisms for a PMN,<sup>11,12</sup> we now propose demagnetization of electrons as a means to release the plasma from the magnetic field. Clearly, as the magnetic nozzle diverges, the magnitude of the magnetic field  $B/B_0$  decays as  $\sim 1/\hat{R}_V^2$  (with  $R_V$  the local nozzle radius). This means that  $\ell_e/\ell_{e0} \sim \hat{R}_V^2$ , and therefore the electron Larmor radius increases fast as the nozzle opens. Typical helicon thrusters,<sup>2,3</sup> have  $\hat{\ell}_{e0}$  in the range  $\sim 10^{-2}$ – $10^{-3}$ , meaning that the electron flow starts to demagnetize roughly at  $R_V \simeq 10$ –30.

Central to this process is the promoted demagnetization in the low- $B$  region, as  $\ell_e$  increases substantially. The value of the electron Larmor radius normalized with its value at the origin,  $\ell_e/\ell_{e0}$ , is portrayed in figure 5. It is apparent that thanks to the induced field, plasma can reach  $\ell_e \sim R$  much earlier for even small values of  $\beta_0$ . Larger values of this parameter increase this effect. This is hence an effective mechanism to facilitate the demagnetization (and thus detachment) of the core of the plasma beam, which contains most of the ion flux. Once demagnetized, the plasma plume will continue to expand under the action of its residual pressure and fields.

Figure 5 also reveals that demagnetization near the plasma edge is not significantly augmented by the plasma induced field, meaning that it will occur approximately at the same zone as in the  $\beta_0 = 0$  case. Again, the small ion flux in this region has a negligible contribution to thrust, and therefore performances would not be noticeably penalized if its detachment occurs further downstream. It might be unavoidable, however, to lose a small fraction of flux due to unsuccessful detachment, which PMN design should minimize. As mentioned above, study of the behavior of the near-edge plasma will require to take into account non-neutral effects.

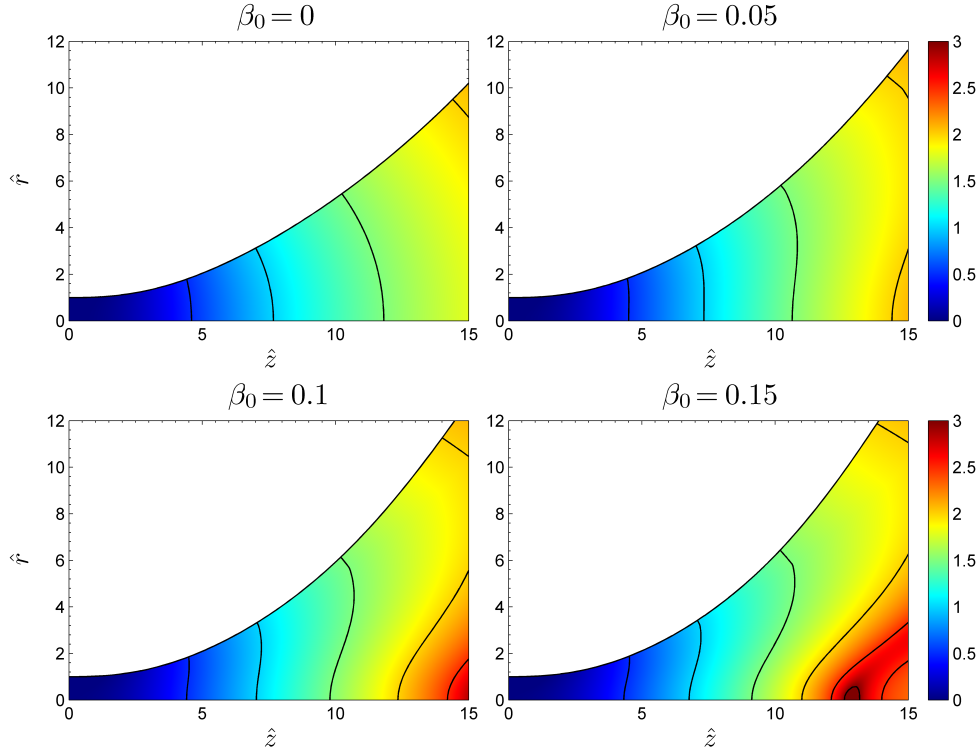


Figure 5. Logarithm of Larmor radius of electrons normalized with its value at the origin,  $\log_{10}(\ell_e/\ell_{e0})$ . Contour lines of this magnitude in steps of 0.5 are shown in black.

## V. Conclusions

By extending our two-dimensional magnetic nozzle model to include the plasma-generated magnetic field, we have confirmed and quantified (1) the increase of nozzle divergence and (2) the diminishing of field intensity induced by the plasma diamagnetic currents. These effects do take place even for very low values of the plasma beta parameter at the origin,  $\beta_0$ . A region of low magnetic field forms about the axis, and it moves upstream for increasing values of  $\beta_0$ . A zero-field point and a separatrix surface occurs in this region for moderate  $\beta_0$ , separating internal and external magnetic fields.

The induced magnetic field is regarded as an excellent mechanism to promote self-demagnetization of the bulk of the plasma beam and attain its detachment. Once the plasma enters the external field region (after separatrix), it can be considered in practice free from the influence of the applied magnetic field. The evolution of the plasma plume thereafter is governed by its residual pressure, currents and fields.

The peripheral plasma carries a very small fraction of the total flux, thanks to the intense rarefaction and self-separation of ion and electron streamtubes close to this border. Induced field does not accelerate demagnetization here, but it can still occur naturally further downstream, as the nozzle opens and  $B$  decreases.

Critical parameters for this process are the initial Larmor Radius-to-nozzle radius ratio,  $\hat{\ell}_{e0}$ , which defines how much  $B/B_{a0}$  needs to decrease in order to achieve demagnetization, and  $\beta_0$ , as it controls the position and shape of the low- $B$  region. Correct design of a PMN will take all these phenomena into account and optimize the value of these parameters in order to detach most of the plasma before the nozzle turning point. In this way, the fraction of plasma lost due to over-attachment and the radial losses can be minimized.

These conclusions are the result of an ongoing research effort, and many aspects of the plasma-field interaction remain our current object of study. Particularly, three points are highlighted: (1) the behavior of the plasma in the low- $B$  region and downstream from the separatrix line. Our current model, based upon perfect electron magnetization, cannot describe a quasi-magnetized plasma. In this highly-complex flow, electron inertia effects (as well as resistivity) need to be taken into account. We are currently working to

include these phenomena into the model.

Additionally, (2) the longitudinal currents arising from the large ion-electron separation in this region might further complicate the flow, and the effects of their azimuthal induced field need to be assessed.

Future work also addresses (3) the investigation of non-neutral effects near the plasma edge, which could play a central role in the detachment of the near-edge plasma flow. This involves the definition of a more precise demagnetization criterion than  $\ell_e \sim R$  or  $\ell_e \sim \lambda_D$ , such as a more refined critical characteristic length and the quantification of electron streamline separation from magnetic streamlines.

## Appendix: Calculation of the Magnetic field

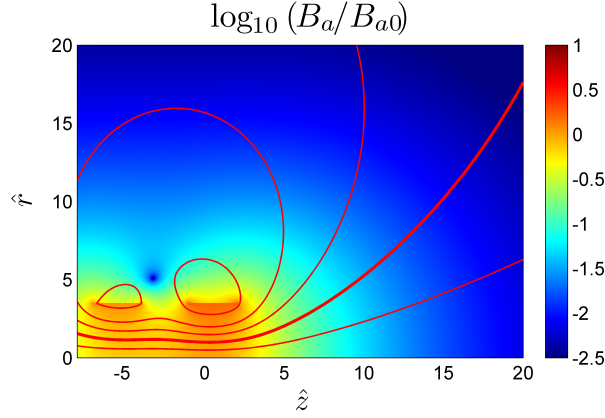


**Figure 6.** Magnetic Field created by the two solenoids, configuration representative for a Helicon thruster. The solenoids have a radius  $\hat{r} = 3.5$ , and run from  $\hat{z} = -7$  to  $-4$ , and from  $-1$  to  $2$ . The field has been normalized with its value at the origin,  $B_{a0}$ . The intensity in the first and second solenoids are in a 4:6 ratio, to provide a stronger field at the open end of the helicon tube. Red lines denote selected magnetic streamlines. The thicker one constitutes the last plasma streamline in the simulations, i.e., the plasma-vacuum edge, and passes through  $\hat{z} = 0$ ,  $\hat{r} = 1$ .

The applied magnetic field  $\mathbf{B}_a$  used for the simulations is generated by two coaxial solenoids, as depicted in figure 6. This configuration is typical of the helicon plasma sources being used for helicon thrusters under development, and is representative of the HPH.com thruster.<sup>4</sup> By using two sets of coils, the resulting magnetic field is quasi-axial inside the helicon quartz tube, and opens at the end to conform a divergent PMN. The magnetic streamfunction  $\psi_a$  and the components  $B_{za}$ ,  $B_{ra}$  of the axisymmetric field can be calculated with the analytical solution of the magnetic field of a single current loop,<sup>21</sup> summing over each loop  $L$ :

$$\psi_a = \sum_L \frac{\mu_0 I_L}{4\pi} \sqrt{(r+r_L)^2 + (z-z_L)^2} [(2-m_L) \mathbf{K}(m_L) - 2\mathbf{E}(m_L)], \quad (13)$$

$$B_{za} = \sum_L \frac{\mu_0 I_L}{2\pi} \frac{1}{\sqrt{(r+r_L)^2 + (z-z_L)^2}} \left[ \mathbf{K}(m_L) - \frac{r^2 - r_L^2 + (z-z_L)^2}{(r-r_L)^2 + (z-z_L)^2} \mathbf{E}(m_L) \right], \quad (14)$$

$$B_{ra} = -\sum_L \frac{\mu_0 I_L}{2\pi r} \frac{(z-z_L)}{\sqrt{(r+r_L)^2 + (z-z_L)^2}} \left[ \mathbf{K}(m_L) - \frac{r^2 + r_L^2 + (z-z_L)^2}{(r-r_L)^2 + (z-z_L)^2} \mathbf{E}(m_L) \right], \quad (15)$$

where  $\mathbf{K}(m)$  and  $\mathbf{E}(m)$  are the complete elliptic integrals of the first and second kind,<sup>22</sup>  $z_L$ ,  $r_L$  denote the intersection of loop  $L$  with a meridional plane,  $I_L$  is the current on each loop (constant for a solenoid), and

$$m_L = \frac{4r_L r}{(r+r_L)^2 + (z-z_L)^2}. \quad (16)$$

The induced magnetic field  $\mathbf{B}_p$ , on the other hand, arises from the plasma response, as electric currents create their own magnetic field. Both azimuthal and longitudinal electric currents exist in the PMN. Since we are interested here in the longitudinal induced field, we are concerned with azimuthal plasma currents,

because they are the only ones generating  $B_{zp}$ ,  $B_{rp}$ . These electric currents are predominantly electron-based, if the plasma has no initial rotation.<sup>10</sup>

The magnitude of the induced field relative to the applied one is characterized by the local plasma beta  $\beta$ , which is proportional to its value at the origin:  $\beta = \mu_0 n T_e / B_a^2 = \beta_0 \hat{n} \hat{B}_{a0}^2 / \hat{B}_a^2$ . This dependence with  $\beta_0$  can be seen from the electron momentum equation,  $0 = -T_e \nabla \ln n + e \nabla \phi - e u_{\theta e} B \mathbf{1}_{\perp}$ , particularized at the nozzle throat where  $\phi = 0$ , and Eq. 10:

$$j_{\theta} \sim \frac{T_e}{B_{a0}}; \quad B_p \sim \beta_0 B_{a0}. \quad (17)$$

Ideally, one would attempt to calculate the induced magnetic field simultaneously with the plasma response, by solving Ampère's equation (Eq. 10), which can be rewritten in terms of the streamfunction  $\psi_p$  ( $B_{zp}$  and  $B_{rp}$  then follow from definitions in Eq. 8),

$$\frac{1}{r} \frac{\partial^2 \psi_p}{\partial z^2} + \frac{\partial}{\partial r} \left( \frac{1}{r} \frac{\partial \psi_p}{\partial r} \right) = \beta_0 B_{a0}^2 n (u_{\theta e} - u_{\theta i}) \quad (18)$$

together with the plasma equations. The field thus obtained would then be added to the applied field to obtain the total magnetic field,  $\mathbf{B} = \mathbf{B}_a + \mathbf{B}_p$ . However, as mentioned in the text, this would break the hyperbolic character of the problem, since Eq. 10 is elliptic in nature (i.e., plasma currents at a given position influence the whole domain), and would force us to abandon the numerous advantages in terms of accuracy and speed associated to the MoC upon which DIMAGNO is based. This argument motivates the iterative approach used to obtain the solution.

A favorable method to calculate the induced magnetic field after concluding each plasma iteration is based on the analytical solution of a single current loop, Eq. 13–15. The obtained distribution of azimuthal current density,  $j_{\theta} dz dr = n (u_{\theta i} - u_{\theta e}) dz dr$ , is discretized at the nodes of a rectangular grid of  $M \times N$  points covering the simulation region. Each node is then treated as a current loop, and the field it creates at the middle points of the grid is calculated analytically using expressions analogous to Eqs. 13–15, producing the “influence matrix” of that current loop in the calculation domain.

The influence of currents inside the plasma source, e.g. an helicon tube, is neglected. This is justified by the small radius of the plasma currents at this point, which means their influence has a limited range, in a region where the applied magnetic field dominates even for moderate values of  $\beta_0$ . Indeed, as it can be appreciated in figure 1, the effect is restricted to a local “leakage” of induced field at the throat region, that would not occur if source currents would be taken into account. Notwithstanding, the influence of these currents is negligible downstream, where detachment and the features under study take place. Similarly, currents beyond a chosen final integration section  $z = z_{MAX}$  need also to be neglected. For the simulations presented in this work,  $z_{MAX} = 20$  was used. It has been checked numerically that the solution for  $z \lesssim 15$  is sufficiently insensitive to the inclusion of currents beyond  $z = 20$ .

Apart from being based on an analytical solution, this approach has the benefit of avoiding the need to use approximate boundary conditions for the calculation domain, which is the main inconvenient of methods based on directly solving Ampère's equation (Eq. 18) numerically, and it also avoids the necessity to numerically differentiate in  $\psi_p$  to obtain  $B_{zp}$  and  $B_{rp}$ , since the magnetic field components can be obtained simultaneously in the same analytical fashion.

By re-using the influence matrix of each loop in a column in an appropriate way, this algorithm has a computational cost in terms of time of the order  $O(MN^2)$ .

## Acknowledgments

This work was sponsored by the Air Force Office of Scientific Research, Air Force Material Command, USAF, under grant number FA8655-10-1-3085. Additional support came from the Gobierno de España (Project AYA-2010-16699). The authors thank I. Martínez for helping with some of the computations.

## References

- <sup>1</sup>Charles, C., Boswell, R. W., and Lieberman, M. A., “Xenon ion beam characterization in a helicon double layer thruster,” *Applied Physics Letters*, Vol. 89, No. 26, 2006, pp. 261503.
- <sup>2</sup>Ziamba, T., Carscadden, J., Slough, J., Prager, J., and Winglee, R., “High Power Helicon Thruster,” *41st AIAA/ASME/SAE/ASEE Joint Propulsion Conference & Exhibit*, AIAA, Washington DC, 2005.

- <sup>3</sup>Batishchev, O., “Minihelicon Plasma Thruster,” *IEEE Transactions on Plasma Science*, Vol. 37, No. 8, Aug. 2009, pp. 1563–1571.
- <sup>4</sup>Pavarin, D., Ferri, F., Manente, M., Curreli, D., Güçlü, Y., Melazzi, D., Rondini, D., Suman, S., Carlsson, J., Bramanti, C., Ahedo, E., Lancellotti, V., and Markelov, G., “Design of 50 W Helicon Plasma Thruster,” *31st International Electric Propulsion Conference*, Electric Rocket Propulsion Society, Fairview Park, OH, 2009.
- <sup>5</sup>Chang-Diaz, F., “An overview of the VASIMR engine: High power space propulsion with RF plasma generation and heating,” *AIP Conference Proceedings*, Vol. 595, AIP, Melville, NY, 2001.
- <sup>6</sup>Krülle, G., Auweter-kurtz, M., and Sasoh, A., “Technology and Application Aspects of Applied Field Magnetoplasma-dynamic Propulsion,” *Journal of Propulsion and Power*, Vol. 14, No. 5, 1998, pp. 754–763.
- <sup>7</sup>Courtney, D. and Martinez-Sanchez, M., “Diverging Cusped-Field Hall Thruster (DCHT),” *30th International Electric Propulsion Conference*, Electric Rocket Propulsion Society, Fairview Park, OH, 2007.
- <sup>8</sup>Raitses, Y., Smirnov, A., and Fisch, N., “Cylindrical Hall Thrusters,” *37th AIAA Plasmadynamics and Lasers Conference*, AIAA, Washington DC, 2006.
- <sup>9</sup>Andersen, S., Jensen, V., Nielsen, P., and D’Angelo, N., “Continuous supersonic plasma wind tunnel,” *Physics of Fluids*, Vol. 12, No. 3, 1969, pp. 557–560.
- <sup>10</sup>Ahedo, E. and Merino, M., “Two-dimensional supersonic plasma acceleration in a magnetic nozzle,” *Physics of Plasmas*, Vol. 17, No. 7, 2010, pp. 073501.
- <sup>11</sup>Ahedo, E. and Merino, M., “Preliminary assessment of detachment in a plasma thruster magnetic nozzle,” *46th AIAA/ASME/SAE/ASEE Joint Propulsion Conference & Exhibit*, AIAA, Washington DC, 2010.
- <sup>12</sup>Ahedo, E. and Merino, M., “On plasma detachment in propulsive magnetic nozzles,” *Physics of Plasmas*, Vol. 18, No. 5, 2011, pp. 053504.
- <sup>13</sup>Arefiev, A. V. and Breizman, B. N., “Magnetohydrodynamic scenario of plasma detachment in a magnetic nozzle,” *Physics of Plasmas*, Vol. 12, No. 4, 2005, pp. 043504.
- <sup>14</sup>Moses Jr, R., Gerwin, R., and Schoenberg, K., “Resistive plasma detachment in nozzle based coaxial thrusters,” *AIP Conference Proceedings*, Vol. 246, AIP, Melville, NY, 1992.
- <sup>15</sup>Hooper, E. B., “Plasma detachment from a magnetic nozzle,” *Journal of Propulsion and Power*, Vol. 9, No. 5, Sept. 1993, pp. 757–763.
- <sup>16</sup>Roberson, B. R., Winglee, R., and Prager, J., “Enhanced diamagnetic perturbations and electric currents observed downstream of the high power helicon,” *Physics of Plasmas*, Vol. 18, No. 5, 2011, pp. 053505.
- <sup>17</sup>Merino, M. and Ahedo, E., “Simulation of plasma flows in divergent magnetic nozzles,” *IEEE Transactions on Plasma Science (accepted)*, 2011.
- <sup>18</sup>Zucrow, M. J. and Hoffman, J. D., *Gas Dynamics, volume I*, John Wiley & sons, 1976.
- <sup>19</sup>Zucrow, M. J. and Hoffman, J. D., *Gas Dynamics, volume II*, Vol. M, John Wiley & sons, 1977.
- <sup>20</sup>Merino, M., Ahedo, E., Bombardelli, C., Urrutxua, H., and Peláez, J., “Hypersonic Plasma Plume Expansion in Vacuum and Preliminary Assessment of Magnetic Effects,” *to be presented in the 32nd International Electric Propulsion Conference*, No. IEPC-2011-086, Electric Rocket Propulsion Society, Fairview Park, OH, 2011.
- <sup>21</sup>Jackson, J., *Classical Electrodynamics*, John Wiley & sons, 2001.
- <sup>22</sup>Abramowitz, M. and Stegun, I., *Handbook of mathematical functions with formulas, graphs, and mathematical tables*, Dover publications, 1964.